

Attitude maneuver of a satellite using movable masses

Liang He^a, Tao Sheng^a, Krishna Dev Kumar^b, Yong Zhao^{a,*}, Dechao Ran^c, Xiaoqian Chen^c



^a College of Aerospace Science and Engineering, National University of Defense Technology, Changsha, 410073, China

^b Department of Aerospace Engineering, Ryerson University, 350 Victoria St., Toronto, Ontario, M5B 2K3, Canada

^c National Innovation Institute of Defense Technology, Beijing, 100081, China

ARTICLE INFO

Keywords:
Spacecraft
Attitude reorientation
Time sub-optimal
Sequence control
Mass shifting

ABSTRACT

This paper investigates the attitude maneuver problem of a spacecraft containing internal movable masses with zero angular momentum. The spacecraft dynamics in one dimension is first studied using the proposed moving mass control system with predefined mass motion. Next, a small-angle attitude maneuver method based on the sliding mode control technique is designed to accomplish the reorientation when the required maneuver angle is within the control capability of single-direction movable mass motion. Furthermore, a novel mass-shifting procedure is proposed for achieving full-domain attitude reorientation. The procedure includes a rest-to-rest maneuver method together with the trajectory optimization. Which, the rest-to-rest maneuver takes advantage of the attitude difference caused by sequential mass motion and the trajectory optimization is carried out based on time sub-optimal motion planning methods. The procedure is next combined with the small-angle maneuver method to achieve a high precision reorientation. Finally, numerical simulation results show that high precision full-domain attitude reorientation can be realized using the proposed control system with three internal movable masses.

1. Introduction

To satisfy the requirements of any space missions, precision pointing control and rapid maneuvering capabilities are two main concerns that need to be considered in designing the control system. Typical actuators used for the system include propulsive devices (e.g., jet thrusters [1]), angular momentum exchanging devices (e.g., reaction wheels [2] and control momentum gyroscopes (CMGs) [3]), and environmental interacting devices (e.g., magnetic torquers [4]). Moving mass control (MMC), by moving several internal masses, can also be used for spacecraft attitude control. The MMC, compared with other control actuators, has three desirable attributes: light weight, simple structure, and low power consumption [5]. Some effects that accompany mass moving include: center of mass (CoM) change, angular momentum exchange, and inertia tensor change, which can be applied properly to tune the spacecraft states.

The effect of CoM change can be used to alter the moment of external force, such as aerodynamic drag [6,7], solar radiation pressure (SRP) [8], or the force produced by jet thrusters [9]. Especially for vehicles operating in dense atmosphere, the aerodynamic drag is unavoidable which attracted a lot of attention in designing the control systems [10–12].

Research of the topic are evidenced in using internal moving mass actuators for attitude and trajectory control of reentry vehicles for the reason that plumes and ablation of the control systems are not need for concern. In the literature, different configurations were presented to complete guidance and control of reentry vehicles. Menon et al. [13] investigated an integrated guidance and control law for a reentry vehicle using three moving masses. Gao et al. [14] proposed a two-loop controller including attitude tracking control and servo control using a single moving mass for the high-speed vehicle. The proposed configuration can experience a roll force as well as the lateral force by adding the ability of rail rotation. Atkins and Queen [15] proposed an LQR-based (Linear Quadratic Regulator) controller with two internal moving mass actuators to track the guidance command for Mars entry. Wang et al. [16] developed a deceleration guidance law for the purpose of avoiding communication blackout using a single moving-mass. Moreover, the masses can also be used in combination with other actuators, such as ailerons and thrusters. Jing et al. [11] proposed a control mode using a single moving mass and differential aileron for long-range reentry vehicle attitude control, which, the aileron is used to get the controllability of the roll channel and an LQR-based controller was proposed to adjust the aileron. Robustness of the system in achieving three-axis attitude control was guaranteed by inducing an extended

* Corresponding author.

E-mail addresses: heliang09@nudt.edu.cn (L. He), shengtao-2002@163.com (T. Sheng), kdkumar@ryerson.ca (K.D. Kumar), zhaoyong@nudt.edu.cn (Y. Zhao), randechao@nudt.edu.cn (D. Ran), chenxiaoqian@nudt.edu.cn (X. Chen).

state observer to eliminate the influence of external disturbances and parameter uncertainties disturbance based on an integrated manner. Meanwhile, the ability to control the roll channel can also be achieved by putting two paired thrusters in a plane. The configuration and control method of using a moving mass in combination with four thrusters was investigated in Ref. [12].

Works using moving masses for attitude stabilization of low-Earth-orbit (LEO) spacecraft also exist in the literature considering cases where aerodynamic torque is the major force or disturbance. Chesi et al. [6,17] investigated control problems when applying movable masses to introduce the aerodynamic torque. In Ref. [17], an adaptive nonlinear feedback control method was proposed with an automatic three sliding-mass balancing simulation system to minimize the distance between the CoM and the center of rotation (CoR) or center of pressure (CoP) which can be applied to eliminate the aerodynamic disturbance. They also used three movable masses for three-axis attitude stabilization, and one reaction wheel or three magnetic torquers were added to make the system fully-actuated [6]. An adaptive nonlinear regulation control law was proposed to generate an ideal torque and then the torque was allocated to the actuators for the stabilization. Virgili-Llop et al. [7] advanced Chesi's concept by considering the complete dynamic model and uncertainties were introduced to the aerodynamic properties in the control process. Moreover, sensitivities of the methods performance with respect to the CoP to CoM distance, spacecraft's size, and orbiting altitude were analyzed. An LQR-based controller was further applied on the two-mass system for pitch and yaw axes while the roll was augmented by an ideal actuator.

Another application of internal mass shifting regards the attitude control of a spacecraft with a large solar sail. Sending the enormous sail directly to space is impossible, thus the deployable solar sail is one of the popular solutions and some pioneering experiments have been carried out [18–20]. The deployed sailcraft, due to its large moment of inertia and disturbance torque created by SRP, presents challenges for conventional control systems. Wie investigated the dynamics and control problem of sailcraft [8,21–23]. As mentioned in Ref. [21], methods to actively control the attitude of the sailcraft include using small reflective vanes or changing the relative location between the CoM and the CoP to get the control torque generated by SRP force. A control system comprising a gimballed control boom with a tip-mounted mass and two or four vanes at the spar tips was proposed to achieve three-axis attitude stabilization [22]. Alternatively, a propellantless primary attitude control system which employs two ballast masses was considered for pitch/yaw control in Ref. [8].

The above-mentioned papers considered the effect of CoM change while the coupling between the masses and the vehicle was ignored as the moving mass considered was relatively small. To address the control method with the coupling effect, Edwards and Kaplan [24] presented equations of motion for an asymmetric rigid spacecraft containing a movable mass and a nonlinear control law was proposed to convert a tumbling spacecraft into simple spin about the major principal axis using the mass. Addressing the same problem, Kunciw and Kaplan [25] proposed an optimal control method that can reduce the time needed to detumble the spacecraft using a single movable mass. Rubenstein and Melton [26] applied direct collocation using nonlinear programming method to attitude reorientation control using two movable appendages which were connected to the main body by three gimbals. Kumar and Zou [27] proposed an LQR-based control law for the attitude stabilization of a miniature satellite using a single movable mass. And our previous work [28] investigated the feasibility of using four movable masses to achieve three-axis attitude stabilization when aerodynamic torque and internal momentum-exchange effect were both considered during the moving mass motion.

In this paper, we are engaged in designing an attitude maneuver method using MMC under zero angular momentum and no external forces assumptions. The controller design represents a challenging problem with the constraint on the displacement of the moving masses with respect to the dimension of a spacecraft. The capability of MMC is

restricted by the mass size and the range of mass motion. Thus, when no external forces can be applied, full-domain attitude reorientation may not be possible as a result of the limited maneuver capability which may explain why few published works emphasize the use of movable masses for attitude maneuver. A system model comprising of a spacecraft with three movable masses is considered for three-axis attitude control in this paper. First, spacecraft dynamics in one dimension with predefined movable mass motion are examined. Second, a movable mass controller based on sliding mode control technique is designed to achieve spacecraft reorientation when the required maneuver angle is within the movable mass control capability. The asymptotic stability of this closed-loop system is proven. Third, a novel mass-shifting procedure is proposed for achieving full-domain attitude reorientation. Trajectory optimization is carried out based on time sub-optimal motion planning methods including eigenaxis rotations. This rest-to-rest maneuver is next combined with the small-angle maneuver method to achieve a high precision reorientation. Compared with the existing works, the main contributions of this paper are summarized as follows:

- 1) Feasibility of full-domain attitude reorientation using internal movable masses is investigated for the first time;
- 2) A novel control procedure using internal movable masses to achieve full-domain attitude reorientation is proposed;
- 3) A high precision reorientation method in a combination of sequence rotation with small angle maneuver is presented.

The paper presents the system dynamics and the controller design, then provides simulation results demonstrating the effectiveness of the proposed method.

2. System model

2.1. Dynamical model of spacecraft with internal mass motion

Assume a spacecraft comprising two parts: a rigid main body m_s and several movable masses m_{pi} (each treated as a point mass). Two coordinate systems are considered (as shown in Fig. 1): an inertial coordinate system $O_X_I Y_I Z_I$, and a body-fixed coordinate system $O_X_b Y_b Z_b$. O represents the center of mass of the main body.

The present investigation considers the attitude reorientation problem using mass-shifting with zero angular momentum. Thus, due to conservation of angular momentum, the equation of motion for a system of connected rigid body is given as

$$\dot{H}_b + \sum_{i=1}^n \mu_i \mathbf{r}_i \times \dot{\mathbf{j}}_i = 0 \quad (1)$$

where \dot{H}_b is the main body angular momentum about its center of mass, μ_i is the reduced mass defined by $\mu_i = \frac{m_{pi}(M - m_{pi})}{M}$, m_{pi} is the mass of the

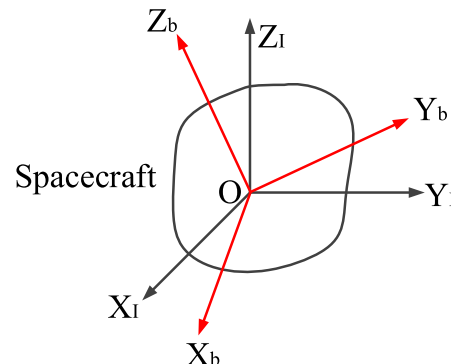


Fig. 1. Coordinate systems.

i-th movable mass, M is the total mass of the spacecraft, and \mathbf{r}_i is the position vector of the i-th mass.

Thus, a force which acts on the control mass is defined as $\mathbf{f}_i = \mu_i \ddot{\mathbf{r}}_i$ and can be expressed in the component form as

$$\begin{aligned} \mathbf{f}_i &= \mu_i \begin{bmatrix} \dot{x}_i \\ \dot{y}_i \\ \dot{z}_i \end{bmatrix} + 2\mu_i \begin{bmatrix} \omega_2 \dot{z}_i - \omega_3 \dot{y}_i \\ \omega_3 \dot{x}_i - \omega_1 \dot{z}_i \\ \omega_1 \dot{y}_i - \omega_2 \dot{x}_i \end{bmatrix} + \mu_i \begin{bmatrix} z_i \dot{\omega}_2 - y_i \dot{\omega}_3 \\ x_i \dot{\omega}_3 - z_i \dot{\omega}_1 \\ y_i \dot{\omega}_1 - x_i \dot{\omega}_2 \end{bmatrix} \\ &+ \mu_i \begin{bmatrix} -x_i(\omega_2^2 + \omega_3^2) + y_i \omega_1 \omega_2 + z_i \omega_1 \omega_3 \\ x_i \omega_1 \omega_2 - y_i(\omega_1^2 + \omega_3^2) + z_i \omega_2 \omega_3 \\ x_i \omega_1 \omega_3 + y_i \omega_2 \omega_3 - z_i(\omega_2^2 + \omega_3^2) \end{bmatrix} \end{aligned} \quad (2)$$

where $\boldsymbol{\omega} = [\omega_1 \ \omega_2 \ \omega_3]^T$ is the angular velocity of the body-fixed coordinate system with respect to the inertial coordinate system and $\mathbf{r}_i = [x_i \ y_i \ z_i]^T$.

Since the main body is rigid, then

$$\dot{H}_b = I\dot{\boldsymbol{\omega}} + \boldsymbol{\omega} \times I\boldsymbol{\omega} \quad (3)$$

where I is the mass moment of inertia matrix of the main body with respect to its center of mass.

Substituting Eqs. (3) and (2) into (1), yields

$$I\dot{\boldsymbol{\omega}} + \boldsymbol{\omega} \times I\boldsymbol{\omega} + \sum_{i=1}^n \mathbf{r}_i \times \mathbf{f}_i = 0 \quad (4)$$

The system considered in this paper is designed as given in Fig. 2. In order to make the system fully actuated, the position vectors of three movable masses \mathbf{m}_{p1} , \mathbf{m}_{p2} and \mathbf{m}_{p3} are set to be $\mathbf{r}_1 = [x_1 \ b \ 0]^T$, $\mathbf{r}_2 = [a \ 0 \ z_2]^T$, $\mathbf{r}_3 = [0 \ b \ z_3]^T$ (as shown in Fig. 2), where a and b are constants depending on the size of the spacecraft and x_1, z_2, z_3 are time-varying. Thus, \mathbf{m}_{p1} moves parallel to the X axis which can control rotation about Z axis, while \mathbf{m}_{p2} can control rotation about the Y axis and \mathbf{m}_{p3} can control rotation about the X axis. All three masses are assumed to be equal, i.e., $m_{pi} = m_p$, $i = 1, 2, 3$.

Suppose that the X, Y, Z axes are principal axes of the rigid main body and $I = \text{diag}(I_{11}, I_{22}, I_{33})$. Then Eq. (4) can be specified as

$$\begin{aligned} \begin{bmatrix} \tilde{I}_1 & -\mu b x_1 & -\mu a z_2 \\ -\mu b x_1 & \tilde{I}_2 & -\mu b z_3 \\ -\mu a z_2 & -\mu b z_3 & \tilde{I}_3 \end{bmatrix} \begin{bmatrix} \dot{\omega}_1 \\ \dot{\omega}_2 \\ \dot{\omega}_3 \end{bmatrix} &= -\begin{bmatrix} \omega_1 \\ \omega_2 \\ \omega_3 \end{bmatrix} \times \begin{bmatrix} \tilde{I}_1 & -\mu b x_1 & -\mu a z_2 \\ -\mu b x_1 & \tilde{I}_2 & -\mu b z_3 \\ -\mu a z_2 & -\mu b z_3 & \tilde{I}_3 \end{bmatrix} \begin{bmatrix} \omega_1 \\ \omega_2 \\ \omega_3 \end{bmatrix} \\ &+ \begin{bmatrix} -\mu b \ddot{z}_3 \\ \mu a \ddot{z}_2 \\ \mu b \ddot{x}_1 \end{bmatrix} + \begin{bmatrix} -2(\mu z_2 \dot{z}_2 + \mu z_3 \dot{z}_3) & 2\mu b \dot{x}_1 & 0 \\ 0 & -2(\mu x_1 \dot{x}_1 + \mu z_2 \dot{z}_2 + \mu z_3 \dot{z}_3) & 0 \\ 2\mu a \dot{z}_2 & 2\mu b \dot{z}_3 & -2\mu x_1 \dot{x}_1 \end{bmatrix} \begin{bmatrix} \omega_1 \\ \omega_2 \\ \omega_3 \end{bmatrix} \end{aligned} \quad (5)$$

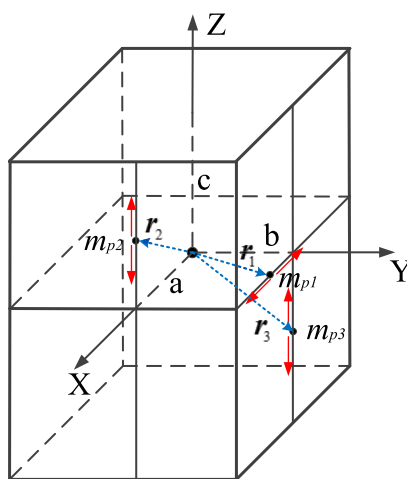


Fig. 2. Distribution of moving masses.

where $\tilde{I}_1 = I_{11} + \mu(2b^2 + z_2^2 + z_3^2)$, $\tilde{I}_2 = I_{22} + \mu(a^2 + x_1^2 + z_2^2 + z_3^2)$, $\tilde{I}_3 = I_{33} + \mu(a^2 + 2b^2 + x_1^2)$.

2.2. Spacecraft one-dimensional motion with predefined movable mass motion

First, the one-dimensional motion of a spacecraft and a movable mass is considered. Set $x_1 \equiv 0$, $z_2 \equiv 0$, then the rotation is a principal axis rotation about the X axis (as shown in Fig. 3). A reduced system can be obtained from Eq. (5) as

$$\tilde{I}_1 \dot{\omega}_1 = -\mu b \ddot{z}_3 - 2\mu z_3 \dot{z}_3 \omega_1 \quad (6)$$

Using Eq. (6), ω_1 is related to z_3 and the first- and second-order derivatives of z_3 , which makes it difficult to find an analytical solution for ω_1 when the movable mass motion is not defined. In order to obtain an analytical solution of ω_1 , the motion of the movable mass is defined as

$$z_3(t) = -A_{z3} \cos(\varepsilon t + \phi) + A_{z3} \quad (7)$$

where A_{z3} is the amplitude of the movable mass motion; ε and ϕ are the angular velocity and phase of the cosine function, respectively.

Assume the initial position is at the origin, i.e., $\phi = 0$. In the rest of this paper, all analyses are based on this predefined motion. Eq. (6) can be solved by applying the predefined motion Eq. (7) using

$$\omega_1 = -\frac{\mu b A_{z3} \varepsilon \sin(\varepsilon t)}{\mu A_{z3}^2 (\cos(\varepsilon t)^2 - 2\cos(\varepsilon t)) + \mu(2b^2 + A_{z3}^2) + I_{11}} \quad (8)$$

Similarly, by setting $x_1 \equiv 0$, $z_3 \equiv 0$ or $z_2 \equiv 0$, $z_3 \equiv 0$, we have

$$\omega_2 = \frac{\mu a A_{z2} \varepsilon \sin(\varepsilon t)}{\mu A_{z2}^2 (\cos(\varepsilon t)^2 - 2\cos(\varepsilon t)) + \mu(a^2 + A_{z2}^2) + I_{22}} \quad (9)$$

$$\omega_3 = \frac{\mu b A_{x1} \varepsilon \sin(\varepsilon t)}{\mu A_{x1}^2 (\cos(\varepsilon t)^2 - 2\cos(\varepsilon t)) + \mu(a^2 + 2b^2 + A_{x1}^2) + I_{33}} \quad (10)$$

Using Eqs. (8) - (10) we can find that ω is a periodic function of time, of which the period is $T = \frac{2\pi}{\varepsilon}$. Assuming that the motion ends in half of the period, then the rotation angle α along the principal axis is obtained as

$$\alpha = \int_0^{T/2} \omega_1 dt \quad (11)$$

Then

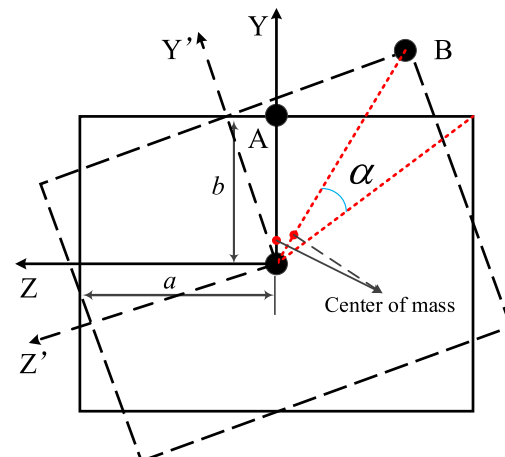


Fig. 3. Illustration of relative rotation between a movable mass and the main body.

$$\alpha \in \begin{cases} \left(-\frac{2\mu b A_{z3}}{2\mu b^2 + 4\mu A_{z3}^2 + I_{11}}, -\frac{2\mu b A_{z3}}{2\mu b^2 + I_{11}} \right) & A_{z3} \leq 0 \\ \left(-\frac{2\mu b A_{z3}}{2\mu b^2 + I_{11}}, -\frac{2\mu b A_{z3}}{2\mu b^2 + 4\mu A_{z3}^2 + I_{11}} \right) & A_{z3} > 0 \end{cases} \quad (12)$$

Referring to Eq. (11), it can be concluded that the rotation angle for half of the period can be determined by the amplitude of the predefined mass motion. Then Eq. (12) is used to obtain the rotation angle for a given amplitude of the predefined mass motion.

It is to be noted that the products of inertia of the spacecraft remain unchanged considering $x_1 \equiv 0$, $z_2 \equiv 0$ in the preceding equations. If $x_1 \equiv a$, $z_2 \equiv c$, Eq. (5) can be expressed as

$$\begin{aligned} & \begin{bmatrix} \tilde{I}_1 & -\mu ab & -\mu ac \\ -\mu ab & \tilde{I}_2 & -\mu bz_3 \\ -\mu ac & -\mu bz_3 & \tilde{I}_3 \end{bmatrix} \begin{bmatrix} \dot{\omega}_1 \\ \dot{\omega}_2 \\ \dot{\omega}_3 \end{bmatrix} = - \begin{bmatrix} \omega_1 \\ \omega_2 \\ \omega_3 \end{bmatrix} \times \begin{bmatrix} \tilde{I}_1 & -\mu ab & -\mu ac \\ -\mu ab & \tilde{I}_2 & -\mu bz_3 \\ -\mu ac & -\mu bz_3 & \tilde{I}_3 \end{bmatrix} \begin{bmatrix} \omega_1 \\ \omega_2 \\ \omega_3 \end{bmatrix} \\ & + \begin{bmatrix} -\mu bz_3 \\ 0 \\ 0 \end{bmatrix} + \begin{bmatrix} -2\mu z_3 \dot{z}_3 & 0 & 0 \\ 0 & -2\mu z_3 \dot{z}_3 & 0 \\ 0 & 2\mu b \dot{z}_3 & 0 \end{bmatrix} \begin{bmatrix} \omega_1 \\ \omega_2 \\ \omega_3 \end{bmatrix} \end{aligned} \quad (13)$$

where $\tilde{I}_1 = I_{11} + \mu(2b^2 + c^2 + z_3^2)$, $\tilde{I}_2 = I_{22} + \mu(2a^2 + c^2 + z_3^2)$, $\tilde{I}_3 = I_{33} + 2\mu(a^2 + b^2)$.

As per the preceding Eq. (13), the rotation is not equal to the principal axis rotation due to the coupling effect.

2.3. Spacecraft kinematics

Using the unit quaternion $q \in R^4$ to describe the spacecraft attitude, the following attitude kinematic equations hold

$$\dot{q}_0 = -\frac{1}{2}\bar{q}^T \omega \quad (14)$$

$$\dot{q} = \frac{1}{2}(q_0 I_{3 \times 3} + \bar{q}^\times)\omega = Q(q)\omega \quad (15)$$

where the unit quaternion is a vector defined by $q = [q_0 \ q_1 \ q_2 \ q_3]^T = [q_0 \ \bar{q}]$ satisfying $\bar{q}^T \bar{q} + q_0^2 = 1$. $\bar{q} \in R^3$ is the vector part while q_0 is the scalar part and $Q(q) = \frac{1}{2}(q_0 I_{3 \times 3} + \bar{q}^\times)$. \bar{q}^\times is the skew-symmetric matrix defined by

$$\bar{q}^\times = \begin{bmatrix} 0 & -a_3 & a_2 \\ a_3 & 0 & -a_1 \\ -a_2 & a_1 & 0 \end{bmatrix} \quad (16)$$

where $a = [a_1 \ a_2 \ a_3]^T$.

The quaternion error is defined by

$$q_e = q_d^{-1} \otimes q = \begin{bmatrix} q_{d0} & q_{d1} & q_{d2} & q_{d3} \\ -q_{d1} & q_{d0} & q_{d3} & -q_{d2} \\ -q_{d2} & -q_{d3} & q_{d0} & q_{d1} \\ -q_{d3} & q_{d2} & -q_{d1} & q_{d0} \end{bmatrix} \begin{bmatrix} q_0 \\ q_1 \\ q_2 \\ q_3 \end{bmatrix} \quad (17)$$

The rotational matrix $R(q)$ between the inertial frame and the body-fixed frame is given by

$$R(q) = (q_0^2 - \bar{q}^T \bar{q})I_{3 \times 3} + 2\bar{q}\bar{q}^T - 2q_0\bar{q}^\times \quad (18)$$

Note that $\|R(q)\| = 1$.

3. Controller design

In the controller design, the following assumptions are made to simplify the theoretical analysis:

Assumption 1. The system properties and dynamics are known.

Assumption 2. The product of inertia change caused by the movable masses is small enough that the rotation caused by mass moving can be

seen as principal rotation.

3.1. Small angle attitude maneuver

Referring to Eq. (12), the small-angle attitude maneuver (within the control capability) can be achieved by moving the masses to a specific position. Here, to ensure that the moving mass motion will not exceed the limitation, we define the small angle as the case where the required maneuver angle is smaller than the lower bound in Eq. (12). A controller for the small-angle attitude maneuver is designed based on the sliding mode control technique. The detailed derivations for the controller design are given next.

Considering Assumption 1 and applying Eq. (15), following Lagrange expression can be obtained from Eq. (4)

$$\tilde{M}\ddot{q}_e + \tilde{C}\dot{q}_e = \tilde{G}^T T_c \quad (19)$$

where the coupling matrices \tilde{C} , \tilde{G} and \tilde{M} are defined as

$$\tilde{G} = Q(\bar{q}_e)^{-1} \quad (20)$$

$$\tilde{M} = \tilde{G}^T I \tilde{G} \quad (21)$$

$$\tilde{C} = -\frac{1}{4}\tilde{M}(\bar{q}_e^\times \tilde{G}\dot{q}_e)^\times \tilde{G} + \frac{1}{4}\tilde{M}(\bar{q}_e^T \tilde{G}\dot{q}_e)\tilde{G} + \tilde{G}^T(\tilde{G}\dot{q}_e)^\times I \tilde{G} \quad (22)$$

$$T_c = -\sum_{i=1}^3 \mathbf{r}_i \times \mathbf{f}_i \quad (23)$$

The controller is designed as

$$T_c = (\tilde{G}^T)^{-1}\tilde{M}(\tilde{M}^{-1}\tilde{C}\dot{q}_e - K_1\dot{q}_e - \eta \text{sgn}(s) - Ks) \quad (24)$$

where $K_1, K \in R^{3 \times 3}$ are constant, diagonal and positive-definite matrices.

Define a sliding mode surface as

$$s = \dot{q}_e + K_1 q_e \quad (25)$$

A candidate Lyapunov function is defined as

$$V = \frac{1}{2}s^T s \quad (26)$$

Combined with Eq. (24), the time derivative of V is calculated as

$$\dot{V} = s^T \dot{s} = s^T (\ddot{q}_e + K_1 \dot{q}_e) \quad (27)$$

$$= s^T (-\tilde{M}^{-1}\tilde{C}\dot{q}_e + \tilde{M}^{-1}\tilde{G}^T T_c + K_1 \dot{q}_e) = -\eta |s| - Ks^2 \leq 0$$

Referring to Eqs. (26) and (27), \dot{V} is negative definite and V is positive-definite for all values of $s \neq 0$. Thus, $s = 0$ is asymptotically stable according to LaSalle's invariance principle [29].

In order to restrain the chattering phenomenon, the saturated function

$$\text{sat}(s) = \begin{cases} 1 & s > \Delta \\ ks & |s| \leq \Delta, k = 1/\Delta \\ -1 & s < \Delta \end{cases} \quad (28)$$

is adopted instead of $\text{sgn}(s)$ in Eq. (24), where Δ is the boundary layer. The switch control is used outside the boundary layer while linear feedback control is considered inside the boundary layer.

3.2. Rest-to-rest full-domain attitude reorientation

If the maneuver angle is larger than the control capability of the one-way single-track mass motion, the positions of the movable masses may exceed the dimension of a spacecraft. Thus, the proposed controller may not be feasible and thus, an additional procedure should be developed to tackle this problem.

3.2.1. Procedure of achieving full-domain attitude reorientation with movable masses

Referring to [Assumption 2](#), the body-axis rotations to B from A can be symbolically denoted by (take $3 \rightarrow 2 \rightarrow 1$ sequence as an example):

$$C_1(\theta_1) \leftarrow C_2(\theta_2) \leftarrow C_3(\theta_3) \quad (29)$$

where $C_i(\theta_i)$ indicates a rotation about the i -th axis of the body-fixed frame with an angle θ_i .

We consider achieving any desired attitude reorientation by moving three masses in different sequences, in a rest-to-rest manner. Using Eq. (29) as an example, if another three corresponding inverse rotations are added to the rotational matrix as (using $3 \rightarrow 2 \rightarrow 1$ sequence):

$$C^{B/A} = C_1(-\theta_1)C_2(-\theta_2)C_3(-\theta_3)C_1(\theta_1)C_2(\theta_2)C_3(\theta_3) \quad (30)$$

and a sequence of the above six rotations ($3 \rightarrow 2 \rightarrow 1 \rightarrow 3 \rightarrow 2 \rightarrow 1$ sequence as an example) defined as one cycle. In this case, the sequence in one cycle is not directly inverse, which implies $C^{B/A}$ is not in $3 \rightarrow 2 \rightarrow 1 \rightarrow 1^- \rightarrow 2^- \rightarrow 3^-$ (negative superscript indicates an inverse rotation), $C^{B/A} \neq I$ is always satisfied.

[Fig. 4](#) is the illustration of the process, the number i shows the position of body axes after the i -th rotation. The initial and final coordinate system are $O - XYZ$ and $O - X'Y'Z'$, respectively. Thus, the attitude difference of these two systems can be obtained from the sequential mass motion.

Using Eq. (30), $C^{B/A}$ is determined by the sequence of different principal rotations and an angle of each rotation (θ_i). In order to achieve any given attitude maneuver, one method is to change three rotation angles to get the desired rotational matrix while the sequence of the rotations remains unchanged. For example, if the sequence $3 \rightarrow 2 \rightarrow 1 \rightarrow 3^- \rightarrow 2^- \rightarrow 1^-$ is selected for a desired attitude \mathbf{q}_d , then the reference rotational matrix C_d will be

$$C_d = R(\mathbf{q}_d)R^{-1}(\mathbf{q}_c) \quad (31)$$

where $R(\mathbf{q}_d)$ is the rotational matrix corresponding to \mathbf{q}_d and calculated from Eq. (18).

By solving the preceding equation, we obtain

$$C_1(-\theta_1)C_2(-\theta_2)C_3(-\theta_3)C_1(\theta_1)C_2(\theta_2)C_3(\theta_3) = C_d \quad (32)$$

Thus, angles $\theta_1, \theta_2, \theta_3$ are the control states of each time step.

Alternatively, another method can be applied by changing the sequence of the rotation together with the sign of the rotation angles if the values of $\theta_1, \theta_2, \theta_3$ are defined ahead of time. Then, several rotation candidates can be obtained and the nearest rotation to the ideal one will be selected among the candidates. If taking 6 rotations as a cycle, there will be $C_6^1 C_4^1 C_2^1 A_3^3 - 48 = 240$ rotation candidates with one set of defined rotation angles θ_1, θ_2 and θ_3 (except for the case that $C^{B/A} = I$).

Both methods have their own advantages; the former approach can provide a precise open-loop control close to the reference trajectory while the latter approach requires only selecting the best sequence within the candidate solutions and it does not involve solving Eq. (32) at each time step.

After the defined cycle along with the motion of movable masses, all three masses have returned to their initial positions while the spacecraft attitude has been changed. Then a new cycle starts with the same initial positions of the movable masses and a different orientation. And the new starting orientation is determined by the rotational matrix $C^{B/A}$. Using this approach, it is possible to achieve full-domain attitude reorientation with the combination of a sequence of cycles.

By involving the control inputs including the mass position and period time, Eq. (30) can be rewritten as

$$C^{B/A} = X_0^{A_{z3}}(T)Y_0^{A_{z2}}(T)Z_0^{A_{x1}}(T)X_{A_{z3}}^0(T)Y_{A_{z2}}^0(T)Z_{A_{x1}}^0(T) \quad (33)$$

where $X_0^{A_{z3}}(T)$ means that m_{p3} , which mainly works on the principal body X axis rotation, moves from 0 to A_{z3} in a given time period T, and $X_{A_{z3}}^0(T)$ implies the inverse motion. $Y_0^{A_{z2}}(T)$ and $Y_{A_{z2}}^0(T)$ refer to the

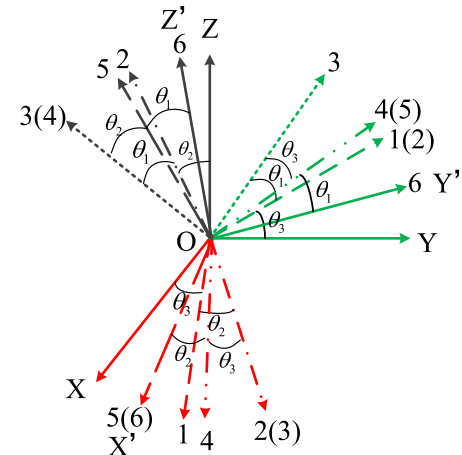


[Fig. 4](#). Illustration of change of body axes in a cycle.

rotation about the principal body Y-axis while $Z_0^{A_{x1}}(T)$ and $Z_{A_{x1}}^0(T)$ represent the rotation about the principal body Z-axis. Note that, without [Assumption 2](#), $Y_0^{A_{z2}}(T), Z_0^{A_{x1}}(T), X_{A_{z3}}^0(T), Y_{A_{z2}}^0(T)$ are not exact principal rotations according to Eq. (13). Solving the corresponding Eq. (33) analytically might not be feasible and thus, we consider the second approach to complete the reorientation, which means each time step is selected within certain rotation candidates.

Since the rotation is a combination of multiple reversible mass motions, the following properties of the rotation candidates can be obtained:

Property 1. If a rotational matrix C is one of the candidates, then C^{-1} is also included in the candidates.

Property 2. $\|C\| = 1$ for every rotational matrix C in the candidates.

Furthermore, how to choose the rotation sequence within the candidates is explained in the next section.

3.2.2. Trajectory optimization

When executing reorientation, the time of maneuver is always a major concern. To choose the appropriate candidate, time-optimal motion planning is considered.

(1) Shortest angular distance rotation

Bilimoria and Wie [30] had proven that the eigenaxis rotation maneuver is not time optimal, but the path solved by eigenaxis rotation has the shortest angular distance [31]. Hence, eigenaxis rotation is adopted to generate a reference attitude trajectory in this paper.

As illustrated in Refs. [32], given a direction cosine matrix $C = [C_{ij}]$, the rotation angle can be found from

$$\cos\theta = \frac{1}{2}(C_{11} + C_{22} + C_{33} - 1) \quad (34)$$

and the eigenaxis \mathbf{e} can be obtained as

$$\mathbf{e} = \begin{bmatrix} e_x \\ e_y \\ e_z \end{bmatrix} = \frac{1}{2\sin\theta} \begin{bmatrix} C_{23} - C_{32} \\ C_{31} - C_{13} \\ C_{12} - C_{21} \end{bmatrix} \quad (35)$$

Dividing the attitude maneuver angle θ into n segments on average, then the unit quaternion of the k-th segment is given by

$$\mathbf{q}_k = \left[\cos \frac{\theta_k}{2} \quad e_x \sin \frac{\theta_k}{2} \quad e_y \sin \frac{\theta_k}{2} \quad e_z \sin \frac{\theta_k}{2} \right]^T \quad (36)$$

where . The n segments form a trajectory for reorientation that represents the shortest angular distance.

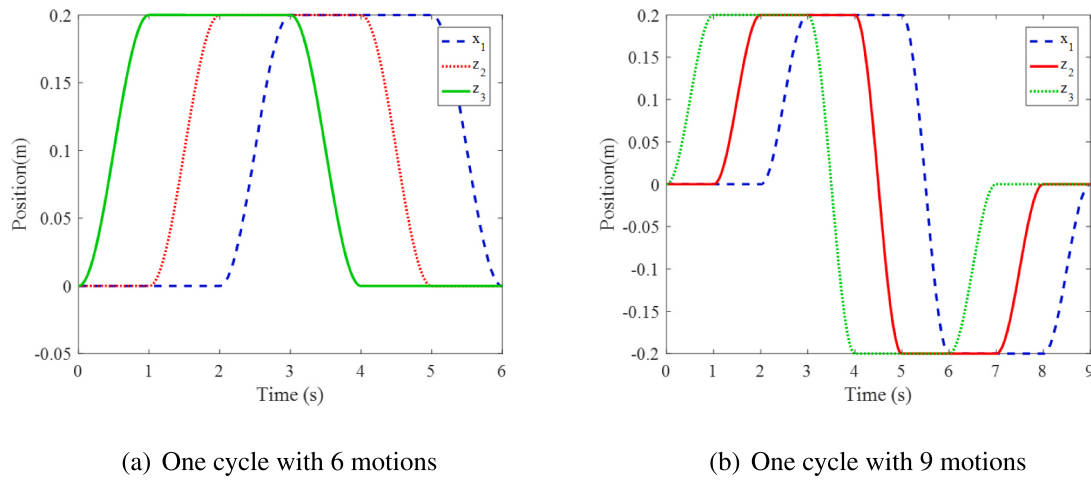


Fig. 5. One cycle with different motions.

(2) Motion planning

In order to reduce the maneuver time, two approaches are considered here; the first approach is based on Eq. (30), where in one cycle is composed of six motions (shown as Fig. 5(a)). The amplitude of the motion of each movable mass is equal to its position limit. The second approach is that one cycle is composed of nine motions (shown as Fig. 5(b)). In the first approach, there are 240 rotation candidates while for the second approach, there are $C_6^1 C_4^1 C_2^1 A_3^3 A_3^3 = 1728$ rotation candidates with one set of defined rotation angles. To get the exact rotational matrix for each candidate, the rotational matrix for each motion is obtained first. These matrices are

$$\begin{aligned}
& R_0^{A_{x1}}(*, 0, 0, T), R_0^{A_{z2}}(0, *, 0, T), R_0^{A_{z3}}(0, 0, *, T), R_0^{\pm A_{x1}}(*, \pm A_{z2}, 0, T) \\
& R_0^{\pm A_{x1}}(*, 0, \pm A_{z3}, T), R_0^{\pm A_{z2}}(\pm A_{x1}, *, 0, T), R_0^{\pm A_{z2}}(0, *, \pm A_{z3}, T), \\
& R_0^{\pm A_{z3}}(\pm A_{x1}, 0, *, T), R_0^{\pm A_{z3}}(0, \pm A_{z2}, *, T), R_0^{\pm A_{x1}}(*, \pm A_{z2}, \pm A_{z3}, T) \\
& R_0^{\pm A_{z2}}(\pm A_{x1}, *, \pm A_{z3}, T), R_0^{\pm A_{z3}}(\pm A_{x1}, \pm A_{z2}, *, T), R_{-A_{x1}}^{A_{x1}} \\
& (*, \pm A_{z2}, \pm A_{z3}, T) \\
& R_{-A_{z2}}^{A_{z2}}(\pm A_{x1}, *, \pm A_{z3}, T), R_{-A_{z3}}^{A_{z3}}(\pm A_{x1}, \pm A_{z2}, *, T)
\end{aligned}$$

where $R_{A_1}^{A_2}(x_1, z_2, z_3, T)$ represents the rotational matrix of the active mass moving from A_1 to A_2 , and the parameters in brackets: * represents the active mass, the other two among the first three parameters are the positions of the static masses (each mass possesses only one degree of freedom), and the last parameter is the time taken for moving from A_1 to A_2 . If these matrices are obtained, a combination of six or nine of them or their inverse provides the rotational matrix of all candidates.

To determine the rotational matrices, a numerical approach is applied with all the properties of the spacecraft assumed to be known. The rotational matrix can be determined by

$$R_{A_1}^{A_2}(x_1, z_2, z_3, T) = R(\mathbf{q}_a)R^{-1}(\mathbf{q}_b) \quad (37)$$

where \mathbf{q}_a and \mathbf{q}_b are quaternions at A_1 and A_2 , respectively.

If there is parameter uncertainty of the given spacecraft, on-orbit calibration could be one of the possible solutions. Eq. (37) can also be used to determine the matrices during the on-orbit calibration. These matrices should be determined before attitude reorientation and after obtaining all the rotation candidates, the reorientation process is completed by solving the following optimization problem:

Find a rotation sequence. $S = \{S(i) \in R_{can}, i = 1, \dots, N\}$

$$\text{Min. } J = \int 1 dt$$

Subject to

$$I\dot{\omega} + \omega \times I\omega + \sum_{i=1}^3 r_i \times f_i = 0 \text{ dynamics}$$

$$\dot{q}_0 = -\frac{1}{2}\bar{q}^T \omega \text{ kinematics}$$

$$\dot{\bar{q}} = \frac{1}{2}(q_0 I_{3 \times 3} + \bar{q}^\times) \omega \text{ kinematics}$$

$$q(t_f) = q_d \text{ boundary}$$

$\omega(t_f) = 0$ boundary

where R_{can} is the set of all rotation candidates and N is the total sequence number.

If the motion within one cycle is not considered, the continuous system becomes a discrete system. The cost function of the discrete system is $J = N$, where N is the number of cycles executed in the process of reorientation. The boundary constraint becomes: $\|\bar{q}_e(t_f)\|_2 \leq \delta$, where δ is the quaternion error bound.

Finding the time optimal solution for the preceding optimization problem takes high computational time, which is not feasible for real time applications. Thus, two time sub-optimal methods are developed to solve the optimization problem. The first method considers the eigenaxis rotation, which involves the shortest angular distance. Then the cost function of this method becomes $J_{k+1} = \|\bar{\mathbf{q}}_{ek_{k+1}}\|_2$, and $\mathbf{q}_{ek_{k+1}} = \mathbf{q}_{k+1}^{-1} \otimes \mathbf{q}_{lk_{k+1}}$, where $\|\cdot\|_2$ is the 2-norm, \mathbf{q}_{k+1} is the $k+1$ th segment of the eigenaxis rotation as in Eq. (36), and $\mathbf{q}_{lk_{k+1}}$ is the $k+1$ th segment of the optimized trajectory. The second method is minimizing the attitude error in each time step while not considering the complete angular distance. Then the cost function of this method becomes $J_{k+1} = \|\bar{\mathbf{q}}_{ek_{k+1}}\|_2$, here $\mathbf{q}_{ek_{k+1}} = \mathbf{q}_d^{-1} \otimes \mathbf{q}_{lk_{k+1}}$, where \mathbf{q}_d is the target orientation.

Here we introduce a lemma to illustrate the feasibility of the preceding two methods.

Lemma 1. If there is a set of rotational matrices, which includes at least two rotational matrices corresponding to quaternions as $\mathbf{q}_{a1} = [q_{a10} \ q_{a11} \ q_{a12} \ q_{a13}]^T$, $\mathbf{q}_{a2} = [q_{a20} \ q_{a21} \ q_{a22} \ q_{a23}]^T$ and satisfy $|\bar{\mathbf{q}}_{a1} \cdot \bar{\mathbf{q}}_{a2}| \leq \frac{1}{2} \|\bar{\mathbf{q}}_{a1}\| \|\bar{\mathbf{q}}_{a2}\|$, with current attitude error $\mathbf{q}_e = [q_{e0} \ q_{e1} \ q_{e2} \ q_{e3}]^T$ satisfies $q_{e0}^2 < \min\{q_{a10}^2, q_{a20}^2\}$, then there will always be a rotational matrix in the candidates that can increase q_{e0}^2 .

Proof. . Since q and $-q$ represent the same attitude, here, we assume $q_0 \geq 0$.

According to Property 1, if $\mathbf{q}_a = [q_{a0} \ q_{a1} \ q_{a2} \ q_{a3}]^T$ is one of the rotation candidates, $\mathbf{q}_b = [q_{a0} \ -q_{a1} \ -q_{a2} \ -q_{a3}]^T$ is also one of the candidates. Then the quaternions after \mathbf{q}_a and \mathbf{q}_b are

$$\mathbf{q}_{ea} = \mathbf{q}_a \otimes \mathbf{q}_e = \begin{bmatrix} q_{e0}q_{a0} - q_{e1}q_{a1} - q_{e2}q_{a2} - q_{e3}q_{a3} \\ q_{e0}q_{a1} + q_{e1}q_{a0} + q_{e2}q_{a3} - q_{e3}q_{a2} \\ q_{e0}q_{a2} - q_{e1}q_{a3} + q_{e2}q_{a0} + q_{e3}q_{a1} \\ q_{e0}q_{a3} + q_{e1}q_{a2} - q_{e2}q_{a1} + q_{e3}q_{a0} \end{bmatrix} \quad (38)$$

$$\mathbf{q}_{eb} = \mathbf{q}_b \otimes \mathbf{q}_e = \begin{bmatrix} q_{e0}q_{a0} + q_{e1}q_{a1} + q_{e2}q_{a2} + q_{e3}q_{a3} \\ -q_{e0}q_{a1} + q_{e1}q_{a0} - q_{e2}q_{a3} + q_{e3}q_{a2} \\ -q_{e0}q_{a2} + q_{e1}q_{a3} + q_{e2}q_{a0} - q_{e3}q_{a1} \\ -q_{e0}q_{a3} - q_{e1}q_{a2} + q_{e2}q_{a1} + q_{e3}q_{a0} \end{bmatrix} \quad (39)$$

Since $q_{e0} < q_{a0} < 1$, together with $\text{norm}(\mathbf{q}_e) = \text{norm}(\mathbf{q}_a) = 1$. Then

$$\begin{aligned} |q_{e0}q_{a0} - q_{e0}| &< |q_{a0}(q_{a0} - 1)| = \frac{q_{a0}}{1 + q_{a0}}(1 - q_{a0}^2) = \frac{q_{a0}}{1 + q_{a0}} |\bar{\mathbf{q}}_a|^2 \\ &\leq \frac{1}{2} |\bar{\mathbf{q}}_a|^2 \end{aligned} \quad (40)$$

Since $|\bar{\mathbf{q}}_{a1}\bar{\mathbf{q}}_{a2}| \leq \frac{1}{2}|\bar{\mathbf{q}}_{a1}||\bar{\mathbf{q}}_{a2}|$, the angle between $\bar{\mathbf{q}}_{a1}$ and $\bar{\mathbf{q}}_{a2}$ satisfies $60^\circ \leq \theta_1 \leq 120^\circ$ (shown in Fig. 6). If $|\bar{\mathbf{q}}_e \cdot \bar{\mathbf{q}}_{a1}| < \frac{1}{2}|\bar{\mathbf{q}}_e||\bar{\mathbf{q}}_{a1}|$, which means $\bar{\mathbf{q}}_e$ lies out of the shadowed zone, then $|\bar{\mathbf{q}}_e \cdot \bar{\mathbf{q}}_{a2}| > \frac{1}{2}|\bar{\mathbf{q}}_e||\bar{\mathbf{q}}_{a2}|$ holds. Thus, $\bar{\mathbf{q}}_{a1}$ and $\bar{\mathbf{q}}_{a2}$ will have at least one of them satisfying $|\bar{\mathbf{q}}_e \cdot \bar{\mathbf{q}}_{ai}| > \frac{1}{2}|\bar{\mathbf{q}}_e||\bar{\mathbf{q}}_{ai}|$, $i = 1, 2$.

Using Eqs. (38) and (39), we obtain

$$(\mathbf{q}_{ea}(1) - q_{e0})(\mathbf{q}_{eb}(1) - q_{e0}) = (q_{e0}q_{a0} - q_{e0} - \bar{\mathbf{q}}_e \cdot \bar{\mathbf{q}}_a)(q_{e0}q_{a0} - q_{e0} + \bar{\mathbf{q}}_e \cdot \bar{\mathbf{q}}_a) \quad (41)$$

Further we have $|\bar{\mathbf{q}}_e \cdot \bar{\mathbf{q}}_a| = |\bar{\mathbf{q}}_e| \cdot |\bar{\mathbf{q}}_a| |\cos\theta| > |\bar{\mathbf{q}}_a|^2 |\cos\theta|$, where θ is the intersection angle between $\bar{\mathbf{q}}_e$ and $\bar{\mathbf{q}}_a$.

Combined with Eq. (40), if $|\cos\theta| \geq \frac{1}{2}$, then $(\mathbf{q}_{ea}(1) - q_{e0})(\mathbf{q}_{eb}(1) - q_{e0}) < 0$, which means that there exists at least one rotation candidate that can increase q_{e0} . Thus, Lemma 1 is proven.

Using Lemma 1 we can conclude that if the candidates comprise at least two rotational matrices of which the quaternion vector parts have an intersection angle between 60° and 120° , the attitude error will converge to the neighborhood of zero using the proposed method. Here, since the rotational candidates are obtained from permutation and combination of single-axis motions, the similarity in each direction should exist which implies that there should always have two candidates satisfying the intersection angle requirement. Moreover, the performance of the proposed method is determined by the property of the rotation candidates (shown in the condition $q_{e0}^2 < \min\{q_{a10}^2, q_{a20}^2\}$ in Lemma 1).

3.3. High precision reorientation

In order to achieve high precision reorientation, the motion planning method in Section 3.2 is combined with the small angle attitude reorientation method proposed in Section 3.1. Initially, the motion planning method is applied to bring the attitude error within the control capability of the movable masses and then the small-angle reorientation method is used to complete the final maneuver.

4. Numerical simulations

To study the effectiveness and performance of the proposed novel control method, several numerical simulations are carried out in MATLAB 2017. The numerical integrator used was the fourth-order Runge-Kutta, the relative and absolute error tolerance for the integration are 10^{-3} and 10^{-6} , respectively. System parameters for the space-craft used in the numerical simulations are shown in Table 1.

The time-varying position parameters of the three masses are bounded as

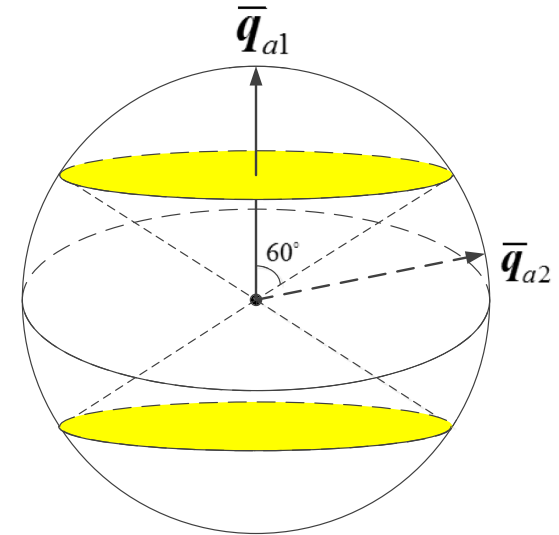


Fig. 6. Orientation relation between $\bar{\mathbf{q}}_{a1}$ and $\bar{\mathbf{q}}_{a2}$

$$\begin{cases} -0.2m \leq x_1 \leq 0.2m \\ -0.2m \leq z_2 \leq 0.2m \\ -0.2m \leq z_3 \leq 0.2m \end{cases} \quad (42)$$

Referring to Eq. (5), when the masses are at their origin, the inertia tensor is $\text{diag}(0.709, 0.875, 0.784)$ and the products of inertia are zero. Take $x_1 = 0.2$, $z_2 = 0.2$ and $z_3 = 0.2$ as an example, then the inertia tensor becomes

$$I_{0,2} = \begin{bmatrix} 0.858 & -0.056 & -0.075 \\ -0.056 & 1.099 & -0.056 \\ -0.075 & -0.056 & 0.858 \end{bmatrix}$$

The products of inertia are relatively small compared with the principal inertias. Thus, we can conclude that the rotation is near principal axis rotation when the masses are moving.

4.1. Small-angle attitude maneuver

By applying Eq. (12), the range of maximum values of control angles (if only one-dimensional motion is considered) is obtained:

$$\begin{cases} \max(|\alpha|) = \max(|\int_0^{T/2} \omega_1 dt|) \in (4.09^\circ, 4.52^\circ) \\ \max(|\beta|) = \max(|\int_0^{T/2} \omega_2 dt|) \in (4.51^\circ, 4.89^\circ) \\ \max(|\gamma|) = \max(|\int_0^{T/2} \omega_3 dt|) \in (3.74^\circ, 4.09^\circ) \end{cases} \quad (43)$$

Eq. (43) can be used to determine whether the reorientation may exceed the position limit as Eq. (42). The initial attitude error is set to $[4^\circ 4.5^\circ -3^\circ 7^\circ]$, and control parameters are chosen as: $K_1 = \text{diag}(2, 2, 2)$, $K = \text{diag}(0.1, 0.1, 0.1)$, $\eta = 0.1$. Simulation results are shown in Fig. 7. Fig. 7(a) shows that with the proposed sliding mode controller, attitude errors converge to zero in less than 3 s while the angular velocity is in the range of $\pm 5^\circ/\text{s}$ (shown as Fig. 7(c)). Fig. 7(b) is the time response of positions of the movable masses. All three masses are bounded within the limits of $\pm 0.2m$, and no overshooting happens during the process, which guarantees that the control capability can not be affected by factors other than the amplitude. The velocity of each moving mass is within $\pm 0.2m/\text{s}$ (shown in Fig. 7(d)) and thus, the system can be controlled.

4.2. Rest-to-rest full-domain attitude reorientation

In Section 3.2, two kinds of cycles are proposed to get the rotation

Table 1
System parameters.

Para	M/kg	m_p/kg	$I_{11}/kg\cdot m^2$	$I_{22}/kg\cdot m^2$	$I_{33}/kg\cdot m^2$	a/m	b/m	c/m
Value	30.0	2.0	0.625	0.800	0.625	0.2	0.15	0.2

candidates. For one cycle with 6 motions, there are 240 rotation candidates, expressed as c1. While for one cycle with 9 motions, expressed as c2, there are 1728 rotation candidates. All the candidates are obtained from numerical analysis. Fig. 8 is the histogram of the Euler angles after one cycle of all the candidates, with the initial attitude is set to [50° 30° 40°]. The results indicate that the maneuver angle is symmetric about the initial angle. Fig. 8(a) shows that the roll attitude varies within $\pm 0.8^\circ$ for c1, while c2 ranges within $\pm 2^\circ$ compared to the initial attitude angle (shown in Fig. 8(b)). Counterparts of pitch attitude are $\pm 2.5^\circ$ for c1, $\pm 5^\circ$ for c2 (shown in Fig. 8(c) and (d)) and of yaw attitude are $\pm 1.25^\circ$ for c1, $\pm 2.5^\circ$ for c2, respectively (shown in Fig. 8(e) and (f)). It can be concluded that the attitude maneuver capability of c2 is twice as c1 or more, which means that c2 is more efficient compared with c1 even based on the number of motions considered.

Thus we apply c2 to finish the maneuver with the goal of minimizing the overall maneuver time. The initial quaternion vector is taken as $\bar{q}_0 = [0.203 \ -0.759 \ -0.532]^T$ while the desired quaternion is $q_d = [0.9 \ 0.1 \ 0.3 \ 0.3]^T$. Figs. 9 and 10 are time responses of quaternion errors and principal axis orientation trajectory when the cost

functions are chosen as $J_{k+1} = \|\bar{q}_{ek+1}\|_2$, $q_{ek+1} = q_d^{-1} \otimes q_{lk+1}$ and $J_{k+1} = \|\bar{q}_{ek+1}\|_2$, $q_{ek+1} = q_{k+1}^{-1} \otimes q_{lk+1}$, respectively. The terminal condition is set to $\|\bar{q}_{ek+1}\|_2 \geq \|\bar{q}_{ek}\|_2$ for all possible q_{ek+1} . In Fig. 9(a), q^* represents the trajectory of eigenaxis rotation, from which we can obtain that the trajectory of q_{e0} , q_{e1} and q_{e2} deviated from the path of the shortest angular distance, while q_{e3} approaches to the target near the eigenaxis rotation for the first motion planning method. Fig. 10 further validates that the planned trajectory is not corresponding to the shortest angular distance (O-shaped points are the planned path). Fig. 9(b) presents the trajectory along the eigenaxis rotation. The shortest angular distance is well tracked. The final quaternion error vector after the last cycle is $\bar{q}_e = [1.86e-4 \ 0.0024 \ 6.74e-4]^T$, which represents the final reorientation error to be approximately 0.29°. The total cycles adopted in the reorientation of the first planning method are 74 cycles while the second approach takes 75 in this simulation case. Furthermore, the trajectory with the shortest angular distance is not time optimal as per Figs. 11 and 12.

Fig. 11 is the distribution of three body axes from view of the +X, +Y and +Z axes after rotating from the same initial attitude using the 1728 rotation candidates. The distribution is symmetrically scattered across four quadrants which provides the possibility to further reduce the error associated with the desired attitude. However, the distribution is not isotropic due to the predefined mass motion and the difference in inertia tensor. The variation is larger on the vertical axis shown in Fig. 11(a) and (c) and indicates greater control capability in the body Y axis which matches with the results shown in Fig. 8.

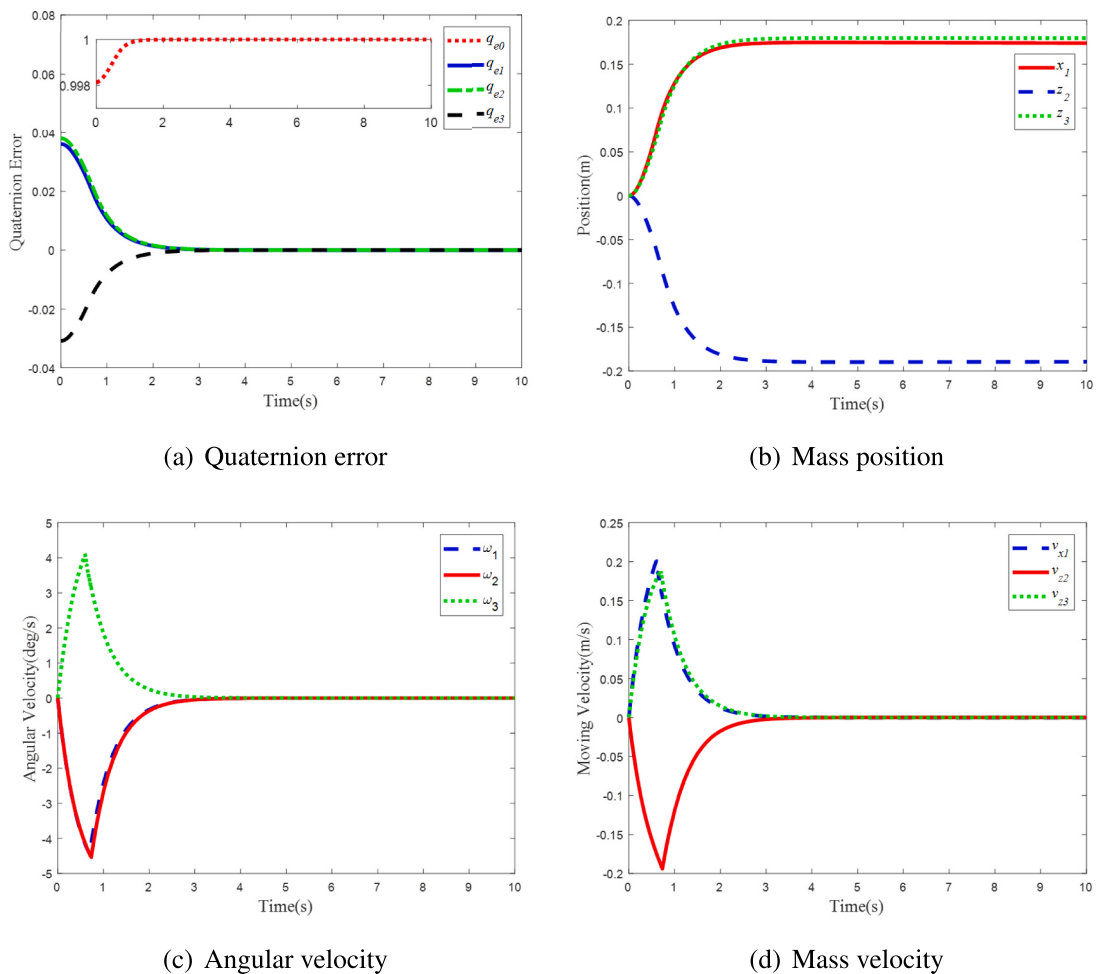


Fig. 7. Time response of the states.

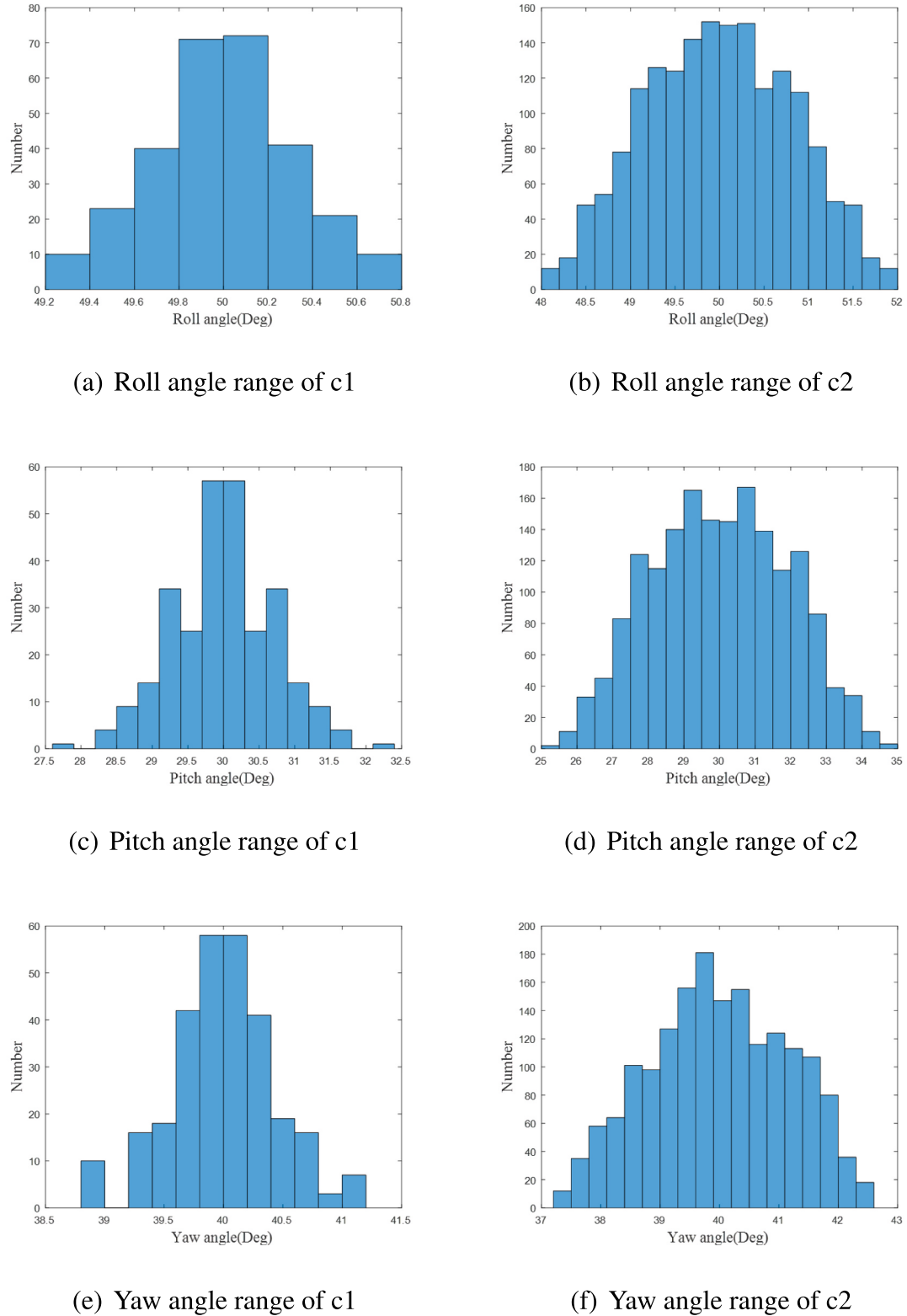


Fig. 8. Histogram of the Euler angles after one cycle of all the candidates.

The motion planning process is demonstrated in Fig. 12. The dot-dashed line represents the shortest distance while the elliptic envelope shows the capability of moving masses at each time step, which can be used to determine the direction of the spacecrafts attitude. Then if the orientation of the shortest distance does not lie in the direction of the

largest capability of the moving masses, it may not be a time-optimal trajectory (as compared with the dashed line). Thus, though eigenaxis rotation represents the shortest angular distance, it may not be the time-optimal trajectory. As a result, this approach is a time sub-optimal motion planning method.

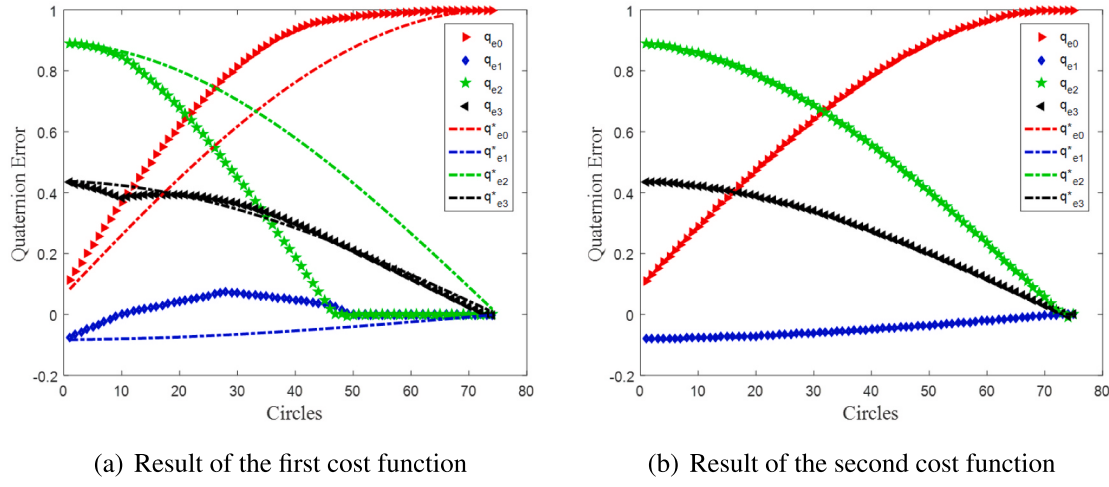


Fig. 9. Time responses of quaternion error using motion planning compared to eigenaxis rotation.

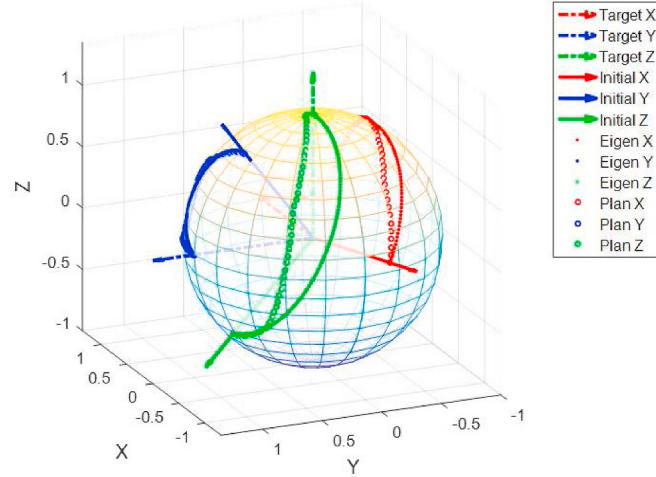


Fig. 10. 3D trajectory comparison of principal axis orientation of the two methods.

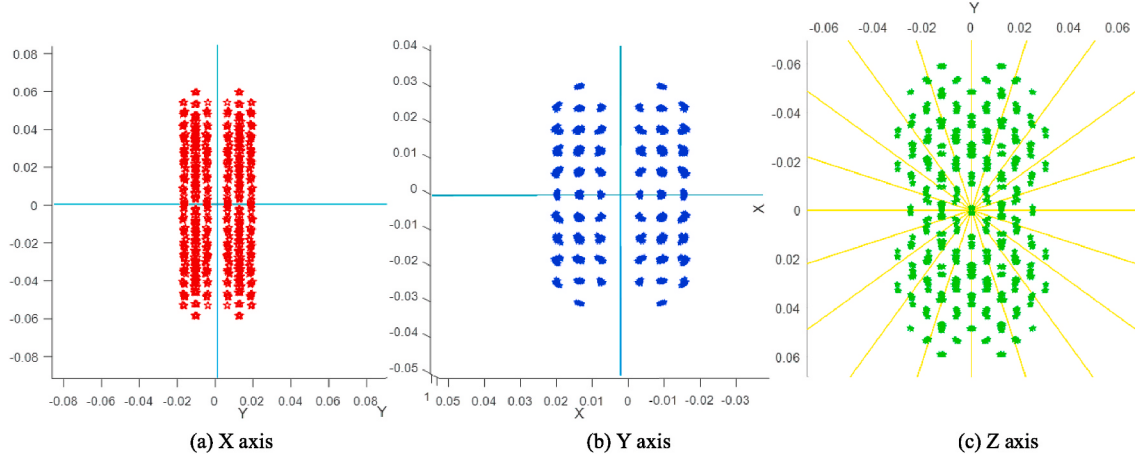


Fig. 11. Three axes orientation of distribution of all candidates of c2.

4.3. High precision reorientation

Figs. 13 and 14 show the results of high precision reorientation proposed in Section 3.3. The terminal condition for sequence control is set to

$\|\bar{q}_{ek+1}\|_2 \leq \varepsilon$, where $\bar{q}_{ek+1} = \mathbf{q}_d^{-1} \otimes \mathbf{q}_{ek+1}$ and ε is determined by the control capability according to Eq. (43). The quaternion error converges to zero in a few seconds as the sequence control ends (see Fig. 13). Fig. 14 indicates that the position is bounded throughout the control procedure.

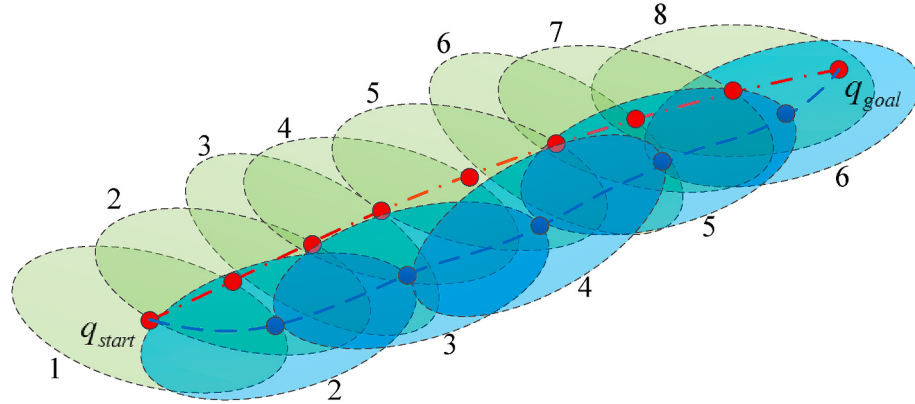


Fig. 12. Demonstration of the motion planning process.

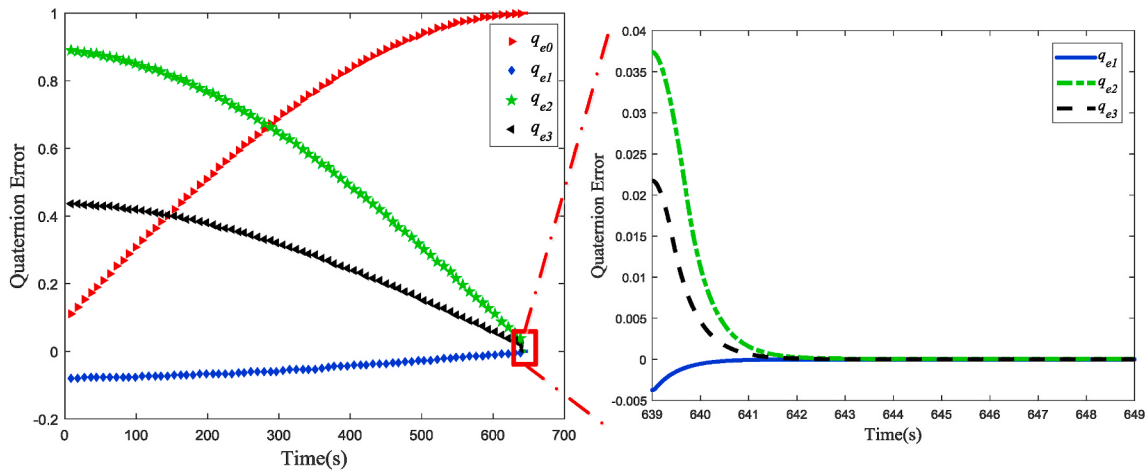


Fig. 13. Time response of quaternion error of high precision reorientation.

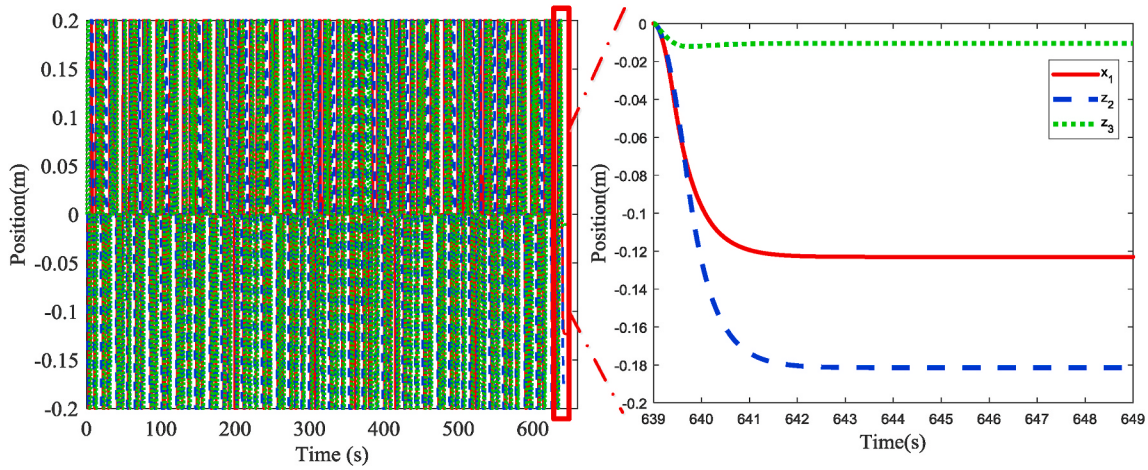


Fig. 14. Time response of three masses position of high precision reorientation.

5. Conclusions

A three-movable-mass-based control system is developed to achieve full-domain attitude reorientation with zero angular momentum. A closed-loop small-angle attitude maneuver method based on a sliding mode controller is designed to accomplish the reorientation when the required maneuver angle is within the control capability of one-directional mass motion. Moreover, a novel mass-shifting procedure is

proposed for realizing full-domain attitude reorientation. Trajectory optimization is carried out based on time sub-optimal motion planning methods. This rest-to-rest control approach is next combined with the small-angle maneuver to achieve a high precision reorientation. The proposed control system can be used for spacecraft where rapid reorientation is not a major concern, such as space observation platforms and deep space explorers.

Further work is needed before implementing the proposed method.

For instance, the rest-to-rest maneuver might have some problems in actual operation and the model uncertainty may affect the possibility of full-domain attitude maneuver. Control methods considering the model uncertainty and performance analysis of the real control system will be considered in our future work.

Declaration of competing interest

The authors declare that they have no known competing financial interests or personal relationships that could have appeared to influence the work reported in this paper.

Acknowledgment

This work was supported by the National Natural Science Foundation of China (Grant no. 11725211).

References

- [1] K. Lemmer, Propulsion for cubesats, *Acta Astronaut.* 134 (2017) 231–243, <https://doi.org/10.1016/j.actaastro.2017.01.048>.
- [2] D. Ran, X. Chen, A. de Ruiter, B. Xiao, Adaptive extended-state observer-based fault tolerant attitude control for spacecraft with reaction wheels, *Acta Astronaut.* 145 (2018) 501–514, <https://doi.org/10.1016/j.actaastro.2018.01.021>.
- [3] V. Lappas, W. Steyn, C. Underwood, Attitude control for small satellites using control moment gyros, *Acta Astronaut.* 51 (1) (2002) 101–111, [https://doi.org/10.1016/S0094-5765\(02\)00089-9](https://doi.org/10.1016/S0094-5765(02)00089-9).
- [4] M. Y. Ovchinnikov, D. Roldugin, A survey on active magnetic attitude control algorithms for small satellites, *Prog. Aero. Sci.* 10 (2016) 0.05.006.
- [5] J. Li, C. Gao, C. Li, W. Jing, A survey on moving mass control technology, *Aero. Sci. Technol.* 82–83 (2018) 594–606, <https://doi.org/10.1016/j.ast.2018.09.033>.
- [6] S. Chesi, Q. Gong, M. Romano, Aerodynamic three-axis attitude stabilization of a spacecraft by center-of-mass shifting, *J. Guid. Contr. Dynam.* 40 (7) (2017) 1613–1626, <https://doi.org/10.2514/1.G002460>.
- [7] J. Virgili-Llop, H.C. Polat, M. Romano, Attitude stabilization of spacecraft in very low earth orbit by center-of-mass shifting, *Frontiers in Robotics and AI* 6 (2019) 7, <https://doi.org/10.3389/frobt.2019.00007>.
- [8] B. Wie, D. Murphy, Solar-sail attitude control design for a flight validation mission, *J. Spacecraft Rockets* 44 (4) (2007) 809–821, <https://doi.org/10.2514/1.22996>.
- [9] A.V. Doroshin, Attitude dynamics of spacecraft with control by relocatable internal position of mass center, *Proceedings of the International MultiConference of Engineers and Computer Scientists*, 2017, pp. 231–235.
- [10] K. Dong, J. Zhou, M. Zhou, B. Zhao, Roll control for single moving-mass actuated fixed-trim reentry vehicle considering full state constraints, *Aero. Sci. Technol.* 94. doi:10.1016/j.ast.2019.105365.
- [11] J. Wuxing, W. Pengxin, G. Changsheng, J. Chunwang, Z. Xu, Roll control analysis for the long-rang reentry vehicle under composite control, 2015 34th Chinese Control Conference (CCC), 2015, pp. 5587–5592, , <https://doi.org/10.1109/ChiCC.2015.7260512>.
- [12] P. Wei, W. Jing, C. Gao, Dynamics and control for hypersonic gliding vehicles equipped with a moving mass and rcs, *J. Aero. Eng.* 32 (5) (2019) 06019003, , [https://doi.org/10.1061/\(ASCE\)AS.1943-5525.0001032](https://doi.org/10.1061/(ASCE)AS.1943-5525.0001032).
- [13] P.K. Menon, G.D. Sweriduk, E.J. Ohlmeyer, D.S. Malyevac, Integrated guidance and control of moving-mass actuated kinetic warheads, *J. Guid. Contr. Dynam.* 27 (1) (2004) 118–126, <https://doi.org/10.2514/1.9336>.
- [14] C. Gao, W. Jing, P. Wei, Research on application of single moving mass in the reentry warhead maneuver, *Aero. Sci. Technol.* 30 (1) (2013) 108–118, <https://doi.org/10.1016/j.ast.2013.07.009>.
- [15] B.M. Atkins, E.M. Queen, Internal moving mass actuator control for mars entry guidance, *J. Spacecraft Rockets* 52 (5) (2015) 1294–1310, <https://doi.org/10.2514/1.A32970>.
- [16] L. Wang, J. Yu, Y. Mei, Y. Wang, Guidance law with deceleration control for moving-mass reentry warhead, *Proc. IME G J. Aero. Eng.* 230 (14) (2016) 0954410016629702, <https://doi.org/10.1177/0954410016629702>.
- [17] S. Chesi, Q. Gong, V. Pellegrini, R. Cristi, M. Romano, Automatic mass balancing of a spacecraft three-axis simulator: analysis and experimentation, *J. Guid. Contr. Dynam.* 37 (1) (2014) 197–206, <https://doi.org/10.2514/1.60380>.
- [18] O. Mori, H. Sawada, R. Funase, M. Morimoto, T. Endo, T. Yamamoto, Y. Tsuda, Y. Kawakatsu, J. Kawaguchi, Y. Miyazaki, Y. Shirasawa, I. D. Team, S. S. W. Group, First solar power sail demonstration by ikaros, transactions of the Japan society for aeronautical and space sciences, *Aerospace Technology Japan* 8 (ists27). doi:10.2322/tastj.8.To_4_25.
- [19] L. Johnson, M. Whorton, A. Heaton, R. Pinson, G. Laue, C. Adams, Nanosail-d: A solar sail demonstration mission, *Acta Astronaut.* 68 (5) (2011) 571–575, <https://doi.org/10.1016/j.actaastro.2010.02.008> special Issue: Aosta 2009 Symposium.
- [20] C. Biddy, T. Svitek, Lightsail-1 solar sail design and qualification, *Proceedings of the 41st Aerospace Mechanisms Symposium*, Jet Propulsion Lab, National Aeronautics and Space Administration Pasadena, CA, 2012, pp. 451–463.
- [21] B. Wie, Solar sail attitude control and dynamics, part 1, *J. Guid. Contr. Dynam.* 27 (4) (2004) 526–535, <https://doi.org/10.2514/1.11134>.
- [22] B. Wie, Solar sail attitude control and dynamics, part two, *J. Guid. Contr. Dynam.* 27 (4) (2004) 536–544, <https://doi.org/10.2514/1.11133>.
- [23] B. Wie, D. Murphy, M. Paluszek, S. Thomas, Robust attitude control systems design for solar sails (part 1): propellantless primary acs, *AIAA Guidance, Navigation, and Control Conference and Exhibit*, 2004, p. 5010, , <https://doi.org/10.2514/6.2004-5010>.
- [24] T.L. Edwards, M.H. Kaplan, Automatic spacecraft detumbling by internal mass motion, *AIAA J.* 12 (4) (1974) 496–502, <https://doi.org/10.2514/3.49275>.
- [25] B. Kuncic, M. Kaplan, Optimal space station detumbling by internal mass motion, *Automatica* 12 (5) (1976) 417–425, [https://doi.org/10.1016/0005-1098\(76\)90003-0](https://doi.org/10.1016/0005-1098(76)90003-0).
- [26] D.S. Rubenstein, R.G. Melton, Multiple rigid-body reorientation using relative motion with constrained final system configuration, *J. Guid. Contr. Dynam.* 22 (3) (1999) 441–446, <https://doi.org/10.2514/2.4416>.
- [27] K.D. Kumar, A.-M. Zou, Attitude control of miniature satellites using movable masses, *SpaceOps 2010 Conference*, AIAA, 2010, , <https://doi.org/10.2514/6.2010-1982>.
- [28] L. He, X. Chen, K.D. Kumar, T. Sheng, C. Yue, A novel three-axis attitude stabilization method using in-plane internal mass-shifting, *Aero. Sci. Technol.* 92 (2019) 489–500, <https://doi.org/10.1016/j.ast.2019.06.019>.
- [29] H.K. Khalil, J.W. Grizzle, *Nonlinear Systems* vol. 3, Prentice hall, Upper Saddle River, NJ, 2002.
- [30] K.D. Bilmoria, B. Wie, Time-optimal three-axis reorientation of a rigid spacecraft, *J. Guid. Contr. Dynam.* 16 (3) (1993) 446–452, <https://doi.org/10.2514/3.21030>.
- [31] R. Xu, H. Wang, W. Xu, P. Cui, S. Zhu, Rotational-path decomposition based recursive planning for spacecraft attitude reorientation, *Acta Astronaut.* 143 (2018) 212–220, <https://doi.org/10.1016/j.actaastro.2017.11.035>.
- [32] B. Wie, *Space Vehicle Dynamics and Control*, American Institute of Aeronautics and Astronautics, 2008.